The effects of 167 MeV Xe^{26+} swift heavy ions irradiation on chemical vapour deposited silicon carbide

T. T. Thabethe[a*], S. A. Adeojo[a,b], M. N. Mirzayev[c,d], V. A. Skuratov[d,e,f], E. G. Njoroge[a,g], O. S. Odutemowo[a], T. T. Hlatshwayo[a]

[a] *Department of Physics, University of Pretoria, Pretoria, South Africa*
[b] *Department of Physics and Engineering Physics, Obafemi Awolowo University, Ile-Ife, Nigeria*
[c] *Institute of Radiation Problems, Azerbaijan National Academy of Sciences, Baku, AZ1143 Azerbaijan*
[d] *Dubna State University, Dubna, Russia*
[e] *Joint Institute for Nuclear Research, Dubna, Russia*
[f] *National Research Nuclear University MEPhI, Moscow, Russia*
[g] *ENGAGE, School of Engineering, University of Pretoria, South Africa*

* *Corresponding author. Email: thabsile.thabethe@up.ac.za*

Abstract

The microstructural changes caused by Xe^{26+} swift heavy ions on polycrystalline SiC were investigated. Chemically vapour deposited SiC samples were irradiated by 167 MeV Xe^{26+} SHI with fluences of 1×10^{12} and 5×10^{14} cm^{-2} at room temperature (RT). The sample composition, phase identification, residual stress and microstructural changes were investigated using X-ray diffraction (XRD) and Raman spectroscopy. The virgin polycrystalline SiC sample was composed of 3C-SiC and 6H-SiC. SHI irradiation caused lattice disorder and lattice expansion. The lattice volume of the SiC samples was observed to increase from 82.2021 $Å^3$ before irradiation to 82.7656 $Å^3$ after irradiating to a fluence of 5×10^{14} cm^{-2}. The SiC sample before and after irradiation had tensile and bi-axial stress which was not homogeneous. The maximum irradiation-induced stress on the SiC microstructure did not exceed 690 MPa after irradiating to the highest fluence.

Keywords: XRD, SHI, residual stress, irradiation, lattice

1. Introduction

The interest in investigating the effects of high energy irradiation, such as swift heavy ion irradiation (SHI) on silicon carbide (SiC), has increased in the past decade. The use of SiC in nuclear environments [1,2] and in the fabrication of sensors (aerospace application) [3–7] which are particularly harsh environments, has sparked this growing interest. In the applications mentioned above, SiC is continuously exposed to irradiation. This irradiation includes ions with energies in the swift heavy ion region, i.e., < 100 MeV/amu. This makes it vital to investigate how these environments affect SiC properties, to what extent the material can withstand the damage when exposed to those conditions, and what kind of damage is introduced to the material.

Over the years, researchers have investigated the effect of SHI irradiation on SiC substrates and on SiC coated with thin metal films [8–12]. Other researchers have investigated the combined effects of SHI irradiation and low energy ion implantation (KeV range) in SiC. Zinkle *et al.* [9] investigated ion tract formation in SiC by irradiating with 245 MeV Kr and 710 MeV Bi ions (swift heavy ions). They reported that SHI irradiation of SiC does not result in track formation. They speculated that the lack of tracks in the SHI irradiated SiC might be due to its high thermal conductivity and that electronic energy loss greater than 34 keV/nm would be required for the track formation in SiC.

Liszkay *et al.* [13] investigated radiation-induced defects in n-type SiC by 246 MeV Kr ion SHI irradiation (fluences ranged from 1×10^{10} cm^{-2} to 1×10^{14} cm^{-2}) using positron measurements. The region they analyzed did not become amorphous, but some defects (vacancy) were created due to the SHI irradiation. The defects created indicated that V_{Si}-V_C divacancy was the dominant trapping site in the implanted region. Other researchers who investigated SiC (doped) structural disorder and point defects/defect formation induced by SHI irradiated at energies above 150 MeV and to different fluences [14–16], reported that the damage caused by the irradiation is in the bulk matrix of the SiC. They further stated that low fluence irradiation results in the SiC retaining its crystalline nature with some damage and high fluence irradiation would result in the sample becoming amorphous. Viswanathan *et al.* [17] stated that SHI irradiation (150 MeV Ag^{12+} ion) results in SiC being partially amorphous with the sublattice damage occurring on the silicon sites. Tunhuma *et al*. [14] confirmed that 167 MeV Xe^{26+} ions irradiation created new defects that were not present before irradiation.

The role of SHI (high energies 167 MeV) in the radiation damage created by ion implantation at low energies (keV) was also reported in some studies [18][15][19]. It was observed that swift heavy ion irradiation of pre-damaged SiC resulted in recrystallization, while irradiation of amorphous SiC resulted in the epitaxial regrowth from the amorphous-crystalline region accompanied by limited recrystallization within the initially amorphous layer. The increase in irradiation fluences results in further recrystallisation (damage removal) in the pre-damaged SiC. From the brief information on the work done on SHI irradiation above, it is clear that a lot of work has indeed been dedicated to understanding the effect of SHI on the SiC at high energies, especially ion track formation, annealing of pre-damage layers and interaction of metal-SiC couples.

Irradiation is known to induce strain in materials which might enhance/hinder interaction between SiC and its surrounding material, thereby reducing the integrity of SiC. There have been some reports which investigated the stress due to irradiation at energies below 1 MeV [20–23] and energies below 100 MeV [24,25]. In all the reports, the swelling of SiC due to irradiation was reported. Szlufarska et al. [25], investigated the role of defects in the swelling and creep of irradiated SiC. This was done by irradiating 4H-SiC with 3.15 MeV C^{2+} ions and 1 MeV Kr^{+} (with irradiation temperatures ranging from RT, 600 °C to 800 °C). The results indicated that the damage profile of the SiC was quasi-flat throughout the entire damage zone, signifying defect saturation. Tensile stress and swelling due to irradiation were reported. The report also indicated that the swelling was observed to reduce due to the defect reduction caused by the increased irradiation temperature. Jankowiak et al. [26] investigated the SiC fiber strain variation in real time after irradiating SiC with 92 MeV Xe ions to a fluence of 5×10^{14} ions cm^{-2}. They reported that irradiation results in the formation of highly disordered SiC and the fiber submitted to a low mechanical loading level of 300 MPa during irradiation did exhibit a gradual increase in its longitudinal strain.

Two main processes (in the nuclear reactor) cause defects/damage to the fuel-coated particle. During the nuclear reactor operation, gases like He, H, etc., which are from light atoms, are released as the first surge of gases within the coated fuel. The second (secondary) wave includes gases from heavy atoms like Xe, Kr, etc. The combination of the first and second waves from the gases will cause defects and induce stress in the protective layers (such as the SiC, which acts as the main diffusion barrier). Thus, this paper investigates the residual stress and microstructural changes caused by 167 MeV Xe^{26+} SHI irradiation to different fluences on SiC substrates. Since the role of SHI irradiation on strain and stress induced in SiC structure at

energies above 100 MeV has not been extensively investigated. This will also add to the already existing knowledge on SHI irradiation of SiC at high energies.

2. Experimental Procedure

In this study, chemical vapour deposited (CVD) polycrystalline SiC wafers from Valley Design Corporation were used. The wafer was cut into 5×5 mm^2 pieces using a diamond scriber. The 5×5 mm^2 SiC pieces were then chemically cleaned (methanol, HF, deionised water) in an ultrasonic bath to remove any contamination. The SiC samples were then irradiated with Xe^{26+} of 167 MeV at room temperature at the Joint Institute for Nuclear Research (JINR), Dubna. The ion fluences were set at 1×10^{12} and 5×10^{14} ions/cm^2. The pristine SiC and the SHI irradiated samples were then analysed using X-ray diffraction (XRD) and Raman spectroscopy.

X-ray diffraction (XRD) was used for phase identification, microstructural changes and residual stress analysis. A Bruker-AXS D8 Advance diffractometer equipped with a theta-theta goniometer then wide-angle X-ray Scattering (WAXS) using a Cu Kα radiation source was used for analysis. The samples were analysed in the two-theta range of 20° to 90° at a step size of 0.04 degree. Measurements were done at 1 sec per step. Primary optics included Goebel mirror for parallel beam and 0.6 mm slit. The phases before and after irradiation were identified using the International Centre for Diffraction Data files (ICDD-PDF-2) database and Match! software.

The average crystallite sizes from the XRD patterns were calculated using the Scherrer equation [27]:

$$\beta = \frac{\lambda k}{L\cos\theta} \tag{1}$$

where β (2θ) is the full width half maximum (FWHM), λ is the wavelength (1.5406 Å), L is the crystallite size, θ is the Bragg angle (in radians) and k is the peak shape factor which is about 0.94 [28].

The concentration of defects in the structure of the samples was studied by calculating the values of lattice strain (ε) and dislocation density (ρ) using equations (2) and (3), respectively [29][30].

$$\varepsilon = \frac{\beta}{4\tan\theta} \tag{2}$$

$$\rho = \frac{1}{D^2} \tag{3}$$

where D is the crystallite size and θ is the Bragg angle. As previously stated, β carries its usual meaning.

For stress, the investigations were performed using a Bruker D8 Discover diffractometer equipped with a theta-2theta goniometer. The instrument was operated in a side-inclination mode. A copper tube (energy = 8 keV) operated in point focus mode was used for the analysis. The primary optics included a 0.8 mm collimator mounted to a graphite monochromator, with no optics on the secondary side. To access the full stress tensor, measurements were carried out at three azimuth angles ϕ, i.e., 0, 45 and 90° with a set of 8 tilt angles in steps of 10° measured for each azimuth angle. To access negative tilt angles, each ϕ was rotated by 180°. To ensure high sensitivity, the SiC (222) reflections at 75.610° (2θ) were selected for the investigations. Measurements were done on two lateral points across the sample surface and the diffracted beam was collected using an area detector, Vantec500. Stress-strain determination was carried out using the manufacturer's proprietary Leptos v6.02 software.

Raman spectroscopy was used to analyse the microstructure of the pristine and the SHI irradiated samples. The Raman equipment used was a WITec alpha 300 RAS+ Confocal micro-Raman microscope equipped with three laser excitation wavelengths. The laser wavelength was 532 nm over a 180 s spectral acquisition time and laser power at 15 mW. The laser penetration depth on the SiC was evaluated using equation (4) [31]:

$$\delta = \frac{1}{2\alpha} \tag{4}$$

where δ is the penetration depth and α is the absorption coefficient. The Raman and XRD data were fitted using the Origin program.

3. Results and discussion

3.1 SRIM Simulation

The Monte Carlo simulation code SRIM-2013 (Stopping and Range of Ions in Matter) [32] was used in full damage cascade mode to simulate the 167 MeV Xe SHIs interaction with the SiC. The density of 3.2 g/cm^3 and displacement energies of 20 and 35 eV for the C and Si, respectively were used for the simulation. Figure 1 shows the energy loss (keV/nm), relative density (%) and the simulated damage in dpa (displacement per atom) of Xe ions as a function

of depth. Figure 1 (a) shows that the electronic energy loss predominates near the surface (with a maximum value of 20.4 keV/nm) up to about 10 µm, rapidly diminishing toward the end of the track. Nuclear energy loss is low close to the surface and has a maximum of 0.3 keV/nm at around 10 µm. This implies that the damage created in the SiC due to the 167 MeV Xe SHI irradiation is mainly due to electronic stopping and only a small fraction of the damage is due to nuclear stopping.

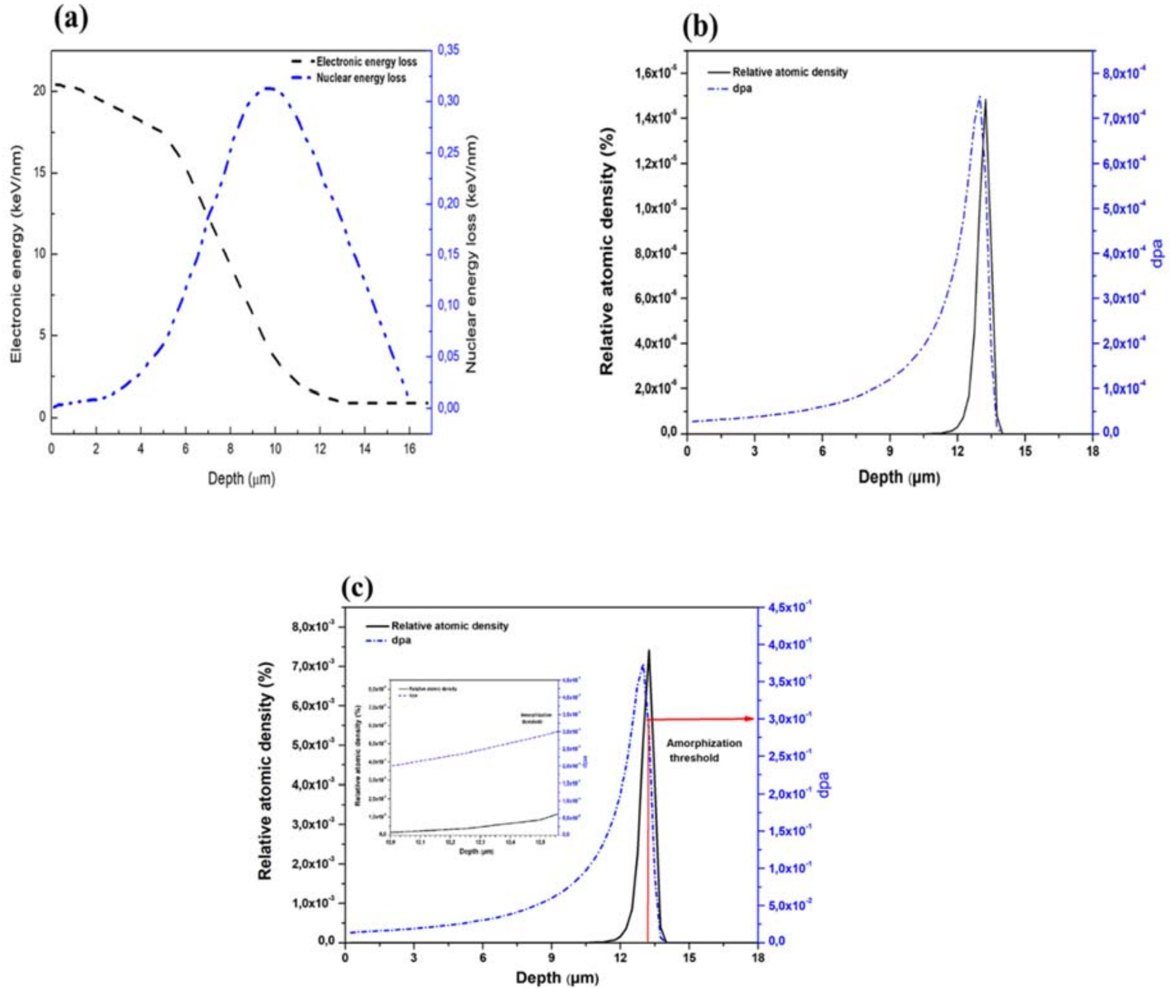

Figure 1: *(a) The SRIM predicted electron and nuclear energy loss depth profile. The relative atomic density (%) of Xe and displacement per atom (dpa) as a function of depth obtained from SRIM simulations for irradiation to fluences (b)* 1×10^{12} *cm*$^{-2}$ *and (c)* 5×10^{14} *cm*$^{-2}$.

Figure 1 (b) shows the SRIM simulation results of the sample irradiated to a fluence of 1×10^{12} cm^{-2} which indicated maximum damage of approximately 7.5×10^{-4} dpa at about 13 µm below

the surface and the simulated projected range was about 13.2 µm. This means that the sample will retain its crystal structure with some degree of radiation damage since it is below the critical damage dose of 0.3 dpa [33]. In Figure 1 (c), the sample irradiated to a fluence of 5×10^{14} cm^{-2} has more damage and at about 0.37 dpa at a depth of about 13 µm below the surface (projected range of 13.3 µm), the samples might sustain a lot of damage. If the amorphization of SiC occurs at 0.3 dpa, it means at a depth of about 12.8 to about 13 µm below the surface, the sample (5×10^{14} cm^{-2}) will be amorphized. The SRIM simulation shows that the sample irradiated to a fluence of 5×10^{14} cm^{-2} will have severe damage compared to the sample irradiated with a fluence of 1×10^{12} cm^{-2}.

3.2 Raman Spectroscopy Analysis

The Raman spectra of the virgin SiC and the samples irradiated with SHIs to fluences of 1×10^{12} cm^{-2} and 5×10^{14} cm^{-2} are shown in Figure 2. The penetration depth for the 532 nm Raman laser was calculated using the equation below [34]:

$$d_p = \frac{2.3}{2\alpha} \qquad (5)$$

where d_p is the penetration depth and α is the absorption coefficient of crystalline SiC (extracted from the values given in ref [34]). The depth penetration was calculated to be about 9.7 microns below the surface of the SiC. This means that the analyzed region in the SiC is limited to the region, where the electronic energy loss is most dominant (as in the SRIM results).

The virgin sample shows the SiC characteristic peaks associated with transversal optical ('TO) mode at approximately 776 cm^{-1}, TO mode at about 803 cm^{-1} and longitudinal optical (LO) mode at approximately 973 cm^{-1}. The peak at 776 cm^{-1} is associated with 6H-SiC and the TO and LO peak at 803 cm^{-1} and 973 cm^{-1} are associated with the 3C-SiC structure. Hence, SiC was composed of both the 3C-SiC and 6H-SiC polytypes. The virgin sample also consists of the second order SiC peak at approximately 1529 cm^{-1} indicating the quality of the wafers [35][36].

Irradiation to a fluence of 1×10^{12} cm^{-2} resulted in the decrease in peak intensity of the SiC peaks accompanied by broadening. Peak shift of the SiC TO and LO modes was also observed to occur from 776 cm^{-1} to 770 cm^{-1} and from 973 cm^{-1} to 970 cm^{-1}, respectively. The TO mode peak at 803 cm^{-1} remained at the same position. A broad peak at approximately 695 cm^{-1} was identified; this peak could be amorphous SiC [37]. The decrease in the peak intensities, peak

broadening and the appearance of a broad (amorphous) SiC peak indicate the presence of damage/lattice distortion within the SiC structure. In addition to these peaks, a Si-Si peak located at around 553 cm^{-1} and a C-C peak at about 1443 cm^{-1} (the so-called D peak) appeared after SHI irradiation to a fluence of 1×10^{12} cm^{-2}.

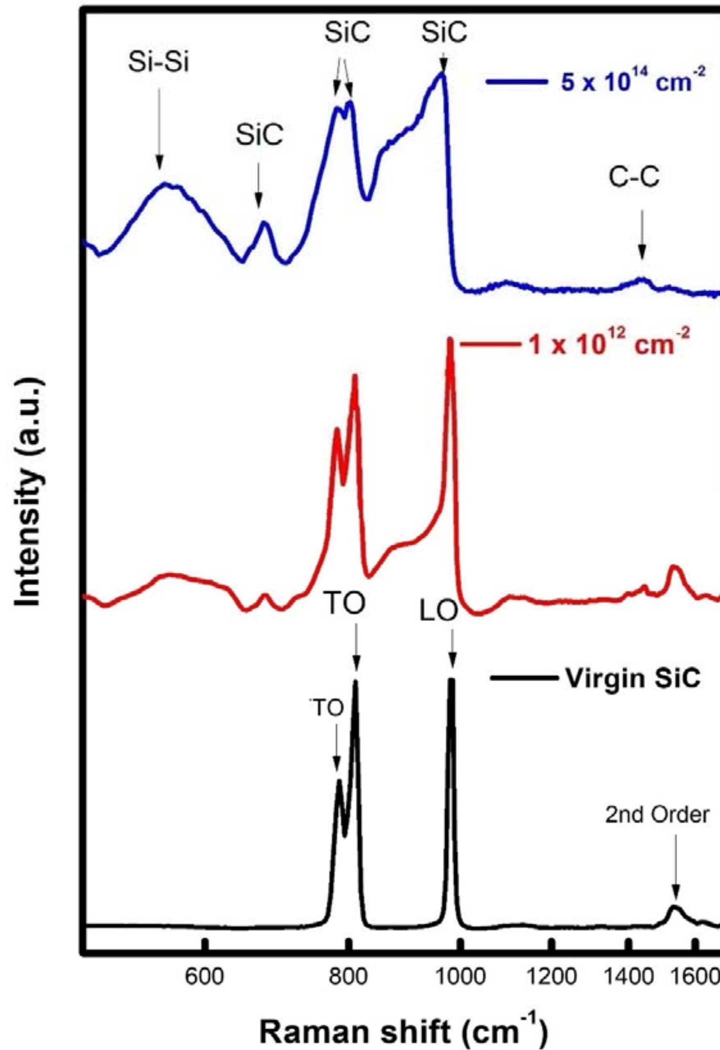

Figure 2: *Raman spectra of CVD SiC before and after SHI irradiation to fluences of* $1\times10^{12}cm^{-2}$ *and* 5×10^{14} cm^{-2}.

Irradiating the SiC sample to the higher fluence of 5×10^{14} cm^{-2} led to a further decrease in the SiC peak intensities. The SiC 'TO, TO and LO peaks shifted to lower wave numbers from 770

cm-1 to 767 cm^{-1}, 803 cm^{-1} to 798 cm^{-1} and 970 to 963 cm^{-1}, respectively. This shift was also accompanied by a significant broadening of the peaks. A pronounced increase in the Si-Si peak intensity at 553 cm^{-1} was also observed, while a slight increase in the C-C peak intensity at 1443 cm^{-1} was observed. The peak located at 1529 cm^{-1} appears to have disappeared. These significant changes to the SiC spectrum after irradiating to a fluence of 5×10^{14} cm^{-2} suggest that there was severe damage sustained in the SiC microstructure compared to the sample irradiated to a fluence of the 1×10^{12} cm^{-2}.

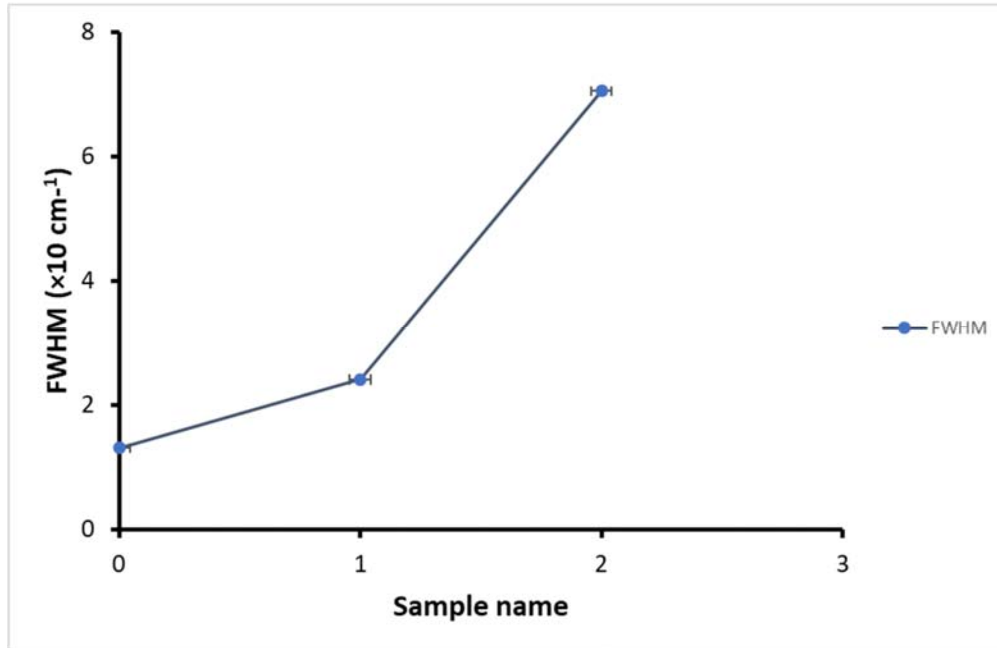

Figure 3: *The LO peak FWHM of the SiC before and after irradiation from the RAMAN data. The samples are represented as follows (0) Virgin SiC, (1)* 1×10^{12} cm^{-2} *and (3)* 5×10^{-14} cm^{-2}.

Si-Si and C-C peaks (after irradiation) can be ascribed to the small population of the displaced Si and C atoms which recoil through the lattice and produce other atomic displacements resulting in a cascade effect and extended radiation damage microstructure [38]. That is, the presence of C-C peaks on Raman is caused by the buildup of interstitial carbon atoms through the condensation of C interstitials generated on the path of irradiated Xe ions [13,39–41]. While the existence of Si–Si bonds may be as a result of the Si atoms contained as the replacement of the carbon atom knocked out by the Xe ion used for irradiation [39]. The Si-Si and C-C bond had broad peaks, indicating partial amorphization on the SiC due to the SHI irradiation. The appearance of the SiC around 695 cm^{-1} was a sign of disordering in the SiC microstructure

(damaged formed within the SiC structure due to the irradiation) [41]. The presence of the Si-Si and C-C and SiC peaks after irradiation also indicates that several nano-crystals are embedded within the SiC structure as a result of irradiation.

The fitted Raman spectra showed an increase in the FWHM of the 'LO' peak present after the samples were irradiated (see Figure 3). The FWHM of the sample irradiation at a fluence of 5×10^{14} cm^{-2} was greater than the one irradiated with a fluence of 1×10^{12} cm^{-2}. The change in the FWHM indicated that they were defects introduced in the SiC material, which resulted in the damaged created on the SiC microstructure. The results show that the sample irradiated at 5×10^{14} cm^{-2} had more damage (higher lattice disorder – amorphous SiC) than the samples irradiated to a fluence of 1×10^{12} cm^{-2}. This is evident from the large peak broadening (increase in FWHM) and decreases in the intensity of the SiC characteristic peaks. The shift is also a sign of swelling characteristics of the irradiated SiC, which was also reported by other researchers [42,43]. The peak shift to lower wavenumbers suggests that the Si-C bond undergoes residual stress (tensile stress) [42,43].

3.3 X-ray Diffraction analysis

XRD analysis was carried out using a wide-angle range to study the structural changes in SiC before and after SHI irradiation. The XRD depth penetration of SiC is between 8 µm and 22 µm [44]. This indicates that the damage created by SHI goes beyond the SRIM predicted region of 13.2 µm. Figure 4 shows XRD pattern of SiC before and after irradiation. The SiC peaks were identified to be at 2θ positions of 35.739° and 75.610°. The SiC peak at 75.610° was 3C-SiC attributed to (222) plane. The peak at position 35.739° with reflections (111) and (222) represented 3C-SiC and 6H-SiC, respectively.

Since the SiC peak for 3C- and 6H-SiC at 35.739° overlay, Rietveld Refinement was done to quantify the phases. Table 1 gives the Rietveld refinement quantification of the phases present in the SiC. The data indicate that the CVD-SiC was composed of 6H-SiC and 3C-SiC. The 3C-SiC was the dominant phase. The virgin sample contained 80 wt% of 3C-SiC and 20 wt% of 6H-SiC. Irradiation of the SiC sample reduced the 3C-SiC composition to 68.9 wt% and increased the 6H-SiC composition to 31.1 wt% at the highest fluence. This indicates that irradiation does affect the phase composition in the SiC.

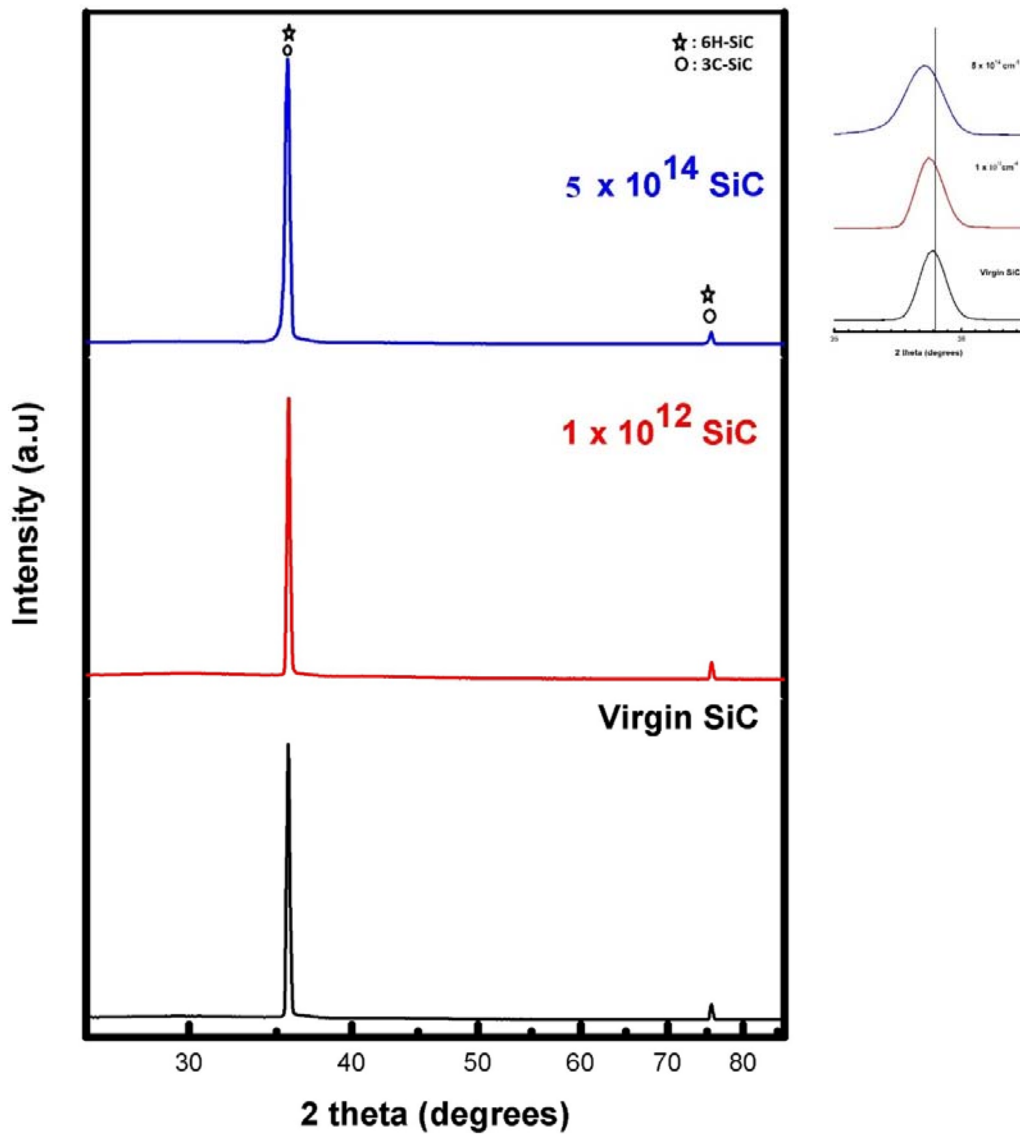

Figure 4: *The CVD SiC XRD pattern before and after irradiation of SiC at 1×10^{12} cm^{-2} and 5×10^{14} cm^{-2} and the insert of the magnified SiC peak around 35.8°.*

From Figure 4, irradiation of the SiC sample to a fluence of 1×10^{12} cm^{-2} resulted in a slight peak shift in both the SiC peaks to a lower 2θ positions. The (111) reflection peaks shifted to 35.701° after 1×10^{12} cm^{-2}. Irradiating the SiC substrate to a fluence of 5×10^{14} cm^{-2} led to further peak shift of the SiC peaks. The (111) reflection peak position was now at 35.655°. The change in the peak position is possibly due to the lattice disorder (lattice expansion) in the crystal structure and the stress introduced by the SHI irradiation [45]. The change in FWHM of the

peaks (peak broadening) was observed. We noted that the peak broadening increased with the irradiation ion fluence. The peak broadening was more evident after irradiation at the highest fluence. This peak broadening is usually a result of nanoparticle effect (*nanocrystalline*) or amorphization and macrostrain [46].

To investigate the crystal structural changes, the change in the average crystallite size was calculated and is presented in Table 2. The average crystallite size of the virgin SiC sample was found to be 32.5 nm. The average crystallite sizes of SiC after irradiating to fluences of 1×10^{12} cm^{-2} and 5×10^{14} cm^{-2} were 31.6 nm and 21.6 nm, respectively. This shows that the peak broadening observed on the SiC XRD pattern was due to the change (decrease) in the crystal size; that is, it was possibly a result of nanoparticle formation caused by the damage introduced by SHI irradiation.

Table 1: shows phase quantification from Rietveld Refinement of CVD SiC.

SiC phase	**Virgin SiC (wt%)**	**1×10^{12} cm^{-2} (wt%)**	**5×10^{14} cm^{-2} (wt%)**
3C	80	73.1	68.9
6H	20	26.9	31.1

The lattice parameter and the cubic unit cell volume before and after SHI irradiation were also calculated. The calculated lattice and volume parameters are shown in Table 2. The results in table 3 indicate that the lattice parameter, *a*, for the SiC increased from (4.3506 ± 0.00024) Å virgin sample to (4.3580 ± 0.000015) Å after irradiating the sample to a fluence of 5×10^{14} cm^{-2}. The increase in the lattice parameter after irradiation is an indication of lattice disorder due to the presence of interstitial defects in the sample. To determine the lattice expansion due to irradiation for SiC, the lattice volume was calculated and is depicted in Table 3. The lattice volume was observed to have changed from (82.3479 ± 0.0145) $Å^3$ (virgin) to (82.7663 ± 0.0009) $Å^3$ at 5×10^{14} cm^{-2}. The increased lattice volume confirmed the lattice swelling (lattice expansion) caused by SHI irradiation.

Table 2: shows the lattice parameter, lattice volume and average crystal size before and after irradiation (for 3C-SiC).

Sample	Lattice parameter, a (Å)	Volume, V (Å^3)	Crystal size (nm)
Virgin	4.3506 ± 0.00024	82.3479 ± 0.0145	32.5
1×10^{12} cm^{-2}	4.3552 ± 0.00031	82.6118 ± 0.0155	31.6
5×10^{14} cm^{-2}	4.3580 ± 0.000015	82.7663 ± 0.0009	21.6

The SiC layers are exposed to some level of lattice strain due to the irradiation and the change in the lattice volume also indicate that the is some level of strain within the SiC lattice structure. Table 3 represents the variation of lattice strain and dislocation density with the change in irradiation fluence. Dislocation density, by definition, is the total length of dislocation lines per unit volume of the crystal [47].

Dislocations are also categorized as the defects in a crystal and they are regions in the crystals where atoms are not orderly aligned. The calculated dislocation values showed an increase in the dislocation's density with the increase in the irradiation fluence. That is, the dislocation density was observed to increase from 0.947×10^{-21} m^{-2} for the virgin SiC to 2.14×10^{-21} m^{-2} after irradiating at a fluence of 5×10^{14} cm^{-2}. The increase in the dislocation density indicates that there was an increase in the level of defects in the SiC layer. The lattice strain calculations indicate that irradiation increases the lattice strain within SiC from 8.95×10^{-4} for the virgin SiC to 13.70×10^{-4} after irradiating at a fluence of 5×10^{14} cm^{-2}. The data shows that the sample sustained a level of deformation due to the SHI irradiation.

Table 3: The strain caused by irradiation on SiC compared to the Virgin SiC calculated from XRD pattern.

Sample	Lattice Strain × 10^{-4}	Dislocation density × 10^{-21} (m^{-2})
Virgin	8.9 ± 2.01	0.95
1 × 10^{12} cm^{-2}	9.9 ± 1.11	1
5 × 10^{14} cm^{-2}	13.7 ± 5.12	2.1

The strain data does support/indicate that there was indeed lattice swelling (volume expansion) due to the defects present in the SiC microstructure.

The residual stress caused by the SHIs irradiation on the SiC substrate was also investigated and it was measured using XRD D8 discover equipment. Table 4 depicts the normal stress components σ_{11} and σ_{22}. The results show that the observed residual stress was tensile and bi-axial for all the samples but did not exceed 690 MPa. The stress on SiC was not homogeneous. The stress along the x-direction (σ_{11}) was more compared to the stress along the σ_{22} y-direction. An increase in tensile stress of the irradiated samples was observed when compared to the virgin SiC sample.

Table 4: *Residual stress and radiation-induced stress on SiC compared with as-deposited samples.*

Irradiation Fluence	Stress components (MPa)		Radiation-induced stress (MPa)	
	σ_{11}	σ_{22}	σ_{11}	σ_{22}
Virgin	438 ± 2.1	433 ± 2.1	-	-
1 × 10^{12} cm^{-2}	498 ± 12.2	470 ± 9.7	60	37
1 × 10^{14} cm^{-2}	673 ± 10.1	668 ± 4.0	240	235

The Raman results indicated a shift in the SiC peak after irradiation and we speculated that it was due to tensile stress (based on previous work done by other researchers[23][48][49]). The XRD data supported the speculation, that is, the stress analysis indicates that the SiC had tensile stress. The results also supported the explanation that the increase in the tensile stress after irradiating is due to the lattice enlargement (increase in the volume parameter). The XRD depth

penetration of SiC is between 8 µm and 22 µm for the SiC [44]. This indicates that the damage created by SHI goes beyond the SRIM predicted region of 13.2 µm.

The XRD and Raman data indicated that the CVD-SiC was composed of 3C-SiC and 6H-SiC. XRD, Rietveld Refinement further indicated that the 3C-SiC (80 wt%) composition was more than the 6H-SiC (20 wt%). XRD and Raman technique analyses are within the damage region as predicted by SRIM simulation and beyond (XRD analysis). The collective results of the damage sustained by the SiC seem to correlate with the SRIM simulation. The Raman results indicated that the SiC sustained a large amount of damage with partial amorphization of the SiC after irradiation. The maximum nuclear energy loss was 0.3 keV/nm, in the nuclear energy region, we expect the SiC to amorphous. The Raman data indicate partial amorphization of SiC, which means the region analyzed also falls part of the Nuclear energy loss region, thus the amorphization was observed on the Raman analysis. In both analyses' technique, the sample irradiated with a fluence of 1×10^{12} cm^{-2} had less damage than the sample irradiated to a fluence of 5×10^{14} cm^{-2}. Other researchers have also reported that irradiating SiC and energies greater than 100 MeV cause significant damage to the SiC [14–17,50], which agrees with our results. The XRD (Rietveld Refinement) also indicated that the 3C-SiCquantity decreases after irradiation and the 6H-SiC quantity increases. The Raman peak intensities of 6H-SiC (around 776 cm^{-1}) and 3C-SiC (around 802 cm^{-1}) were also observed to change after irradiation. That is, the 3C-SiC intensity decreased while the 6H-SiC intensity increased, which was an indication that irradiation does influence the changes in the phases present.

4. Conclusion

The effect of Xe^{26+} swift heavy ion irradiation on SiC to two different fluences (1×10^{12} cm^{-2} and 5×10^{14} cm^{-2}) at room temperatures was investigated. The microstructural changes in the surface and bulk of the SiC samples were studied using XRD and Raman spectroscopy. Moreover, the residual stress was deduced from the XRD data. The Raman analysis of the virgin SiC sample showed that the CVD prepared SiC was composed of two polytypes of SiC, that is, 6H-SiC and 3C-SiC.

The samples irradiated to fluences of 1×10^{12} cm^{-2} and 5×10^{14} cm^{-2} had damage from the surface to the bulk, with more damaged sustained by the sample irradiated at a fluence of 5×10^{14} cm^{-2}. Raman data indicated that SiC became partially amorphized after irradiation. The lattice parameter of the sample changed from 4.3480 Å (virgin SiC) to 4.3579 Å (5×10^{14} cm^{-2}) for

the 3C-SiC polytype indicating lattice distortion (lattice damage) due to the interstitial defects. A change in the volume parameter induced by the irradiation was also reported. The increase in the lattice volume from 82.2021Å^3 (virgin) to 82.7656 Å^3 (5×10^{14} cm^{-2}), indicated that the was lattice swelling. The SiC sample before and after irradiation had tensile and bi-axial stress which was not homogeneous. The residual stresses on the SiC microstructure did not exceed 690 MPa after irradiating with the highest fluence. The increase in the tensile stress due to irradiation was observed.

The appearance of the Si-Si and C-C peak was explained to be due to the small population of the displaced Si and C atoms which recoil through the lattice and produce other atomic displacements resulting in a cascade effect and extended radiation damage microstructure. That is, the presence of C-C peaks on Raman is caused by the buildup of interstitials carbon through the condensation of C interstitials generated on the path of irradiated Xe ions. While the existence of Si–Si bonds is possibly as a result of the Si atoms contained as the replacement of the carbon atom knocked out by the Xe ion used for irradiation.

5. Acknowledgments

The authors wish to thank Dr T. Ntsoane from NECSA for his assistance with XRD data collection and Dr Z.A.Y. Abdalla for assisting with the SRIM simulation. This work is based upon the research supported by the National Research Foundation (NRF) of South Africa (Grant number: 132125). Any opinion, findings, conclusions, or recommendations expressed in this work are those of the authors and the NRF do not accept any liability regarding thereto. T. T. Thabethe acknowledges the financial support from the NRF.

6. References

[1] L. Zhang, W. Jiang, C. Pan, R.C. Fadanelli, W. Ai, L. Chen, T. Wang, Raman study of amorphization in nanocrystalline 3C–SiC irradiated with C+ and He+ ions, J. Raman Spectrosc. 50 (2019) 1197–1204. https://doi.org/10.1002/jrs.5631.

[2] H. Kishimoto, T. Shibayama, T. Abe, K. Shimoda, S. Kawamura, A. Kohyama, Diffusion Bonding Technology of Tungsten and SiC/SiC Composites for Nuclear Applications, IOP Conf. Ser. Mater. Sci. Eng. 18 (2011) 162015. https://doi.org/10.1088/1757-899X/18/16/162015.

[3] H. Gu, Z. Wang, Y. Hu, Hydrogen Gas Sensors Based on Semiconductor Oxide Nanostructures, 2012. https://doi.org/10.3390/s120505517.

[4] K. Kim, G. Chung, Sensors and Actuators B : Chemical Fast response hydrogen sensors based on palladium and platinum / porous 3C-SiC Schottky diodes, Sensors Actuators B. Chem. 160 (2011) 1232–1236. https://doi.org/10.1016/j.snb.2011.09.054.

[5] C.K. Kim, J.H. Lee, Y.H. Lee, N.I. Cho, D.J. Kim, W.P. Kang, Hydrogen Sensing Characteristics of Pd-SiC Schottky Diode Operating at High Temperature, 28 (1999) 202–205.

[6] N.A. And, S. Administration, Advanced Hydrogen and Hydrocarbon Gas Sensors, (n.d.). https://technology.nasa.gov/patent/LEW-TOPS-112 (accessed July 9, 2021).

[7] G.W. Hunter, P.G. Neudeck, D. Makel, C.C. Liu, B. Ward, Q.H. Wu, V. Thomas, P. Dutta, M. Frank, J. Trimbol, M. Fulkerson, B. Patton, Development of Chemical Sensor Arrays for Harsh Environments and Aerospace Applications, Proc. IEEE Sensors. 1 (2002) 1126–1133. https://doi.org/10.1109/icsens.2002.1037272.

[8] A. Benyagoub, A. Audren, Mechanism of the swift heavy ion induced epitaxial recrystallization in predamaged silicon carbide, J. Appl. Phys. 106 (2009). https://doi.org/10.1063/1.3236627.

[9] S.J. Zinkle, J.W. Jones, V.A. Skuratov, Microstructure of swift heavy ion irradiated SiC, Si3N4 and AlN, Mater. Res. Soc. Symp. - Proc. 650 (2001) 1–6. https://doi.org/10.1557/proc-650-r3.19.

[10] S. Sorieul, J.M. Costantini, L. Gosmain, L. Thomé, J.J. Grob, Raman spectroscopy study of heavy-ion-irradiated α-SiC, J. Phys. Condens. Matter. 18 (2006) 5235–5251. https://doi.org/10.1088/0953-8984/18/22/022.

[11] T.T. Thabethe, T.P. Ntsoane, S. Biira, E.G. Njoroge, T.T. Hlatshwayo, V.A. Skuratov, J.B. Malherbe, Investigating the structural changes induced by SHI on W–SiC samples, Vacuum. 174 (2020). https://doi.org/10.1016/j.vacuum.2020.109230.

[12] E.G. Njoroge, C.C. Theron, V.A. Skuratov, D. Wamwangi, T.T. Hlatshwayo, C.M. Comrie, J.B. Malherbe, Interface reactions between Pd thin films and SiC by thermal annealing and SHI irradiation, Nucl. Instruments Methods Phys. Res. Sect. B Beam Interact. with Mater. Atoms. 371 (2016) 263–267.

https://doi.org/10.1016/j.nimb.2015.10.014.

[13] L. Liszkay, K. Havancsák, M.F. Barthe, P. Desgardin, L. Henry, Z. Kajcsos, G. Battistig, E. Szilágyi, V.A. Skuratov, Swift heavy ion irradiation effects in SiC measured by positrons, Mater. Sci. Forum. 363–365 (2001) 123–125. https://doi.org/10.4028/www.scientific.net/msf.363-365.123.

[14] S.M. Tunhuma, M. Diale, J.M. Nel, M.J. Madito, T.T. Hlatshwayo, F.D. Auret, Defects in swift heavy ion irradiated n-4H-SiC, Nucl. Instruments Methods Phys. Res. Sect. B Beam Interact. with Mater. Atoms. 460 (2019) 119–124. https://doi.org/10.1016/j.nimb.2018.11.046.

[15] T.T. Hlatshwayo, J.H. O'Connell, V.A. Skuratov, M. Msimanga, R.J. Kuhudzai, E.G. Njoroge, J.B. and Malherbe, Effect of Xe ion (167 MeV) irradiation on polycrystalline SiC implanted with Kr and Xe at room temperature, J. Phys. D. Appl. Phys. 48 (2015) 465306. https://doi.org/10.1088/0022-3727/48/46/465306.

[16] T.T. Thabethe, T. Nstoane, S. Biira, E.G. Njoroge, T.T. Hlatshwayo, V.A. Skuratov, J.B. Malherbe, Irradiation effects of swift heavy ions on palladium films deposited on 6H-SiC substrate, Nucl. Instruments Methods Phys. Res. Sect. B Beam Interact. with Mater. Atoms. 442 (2019). https://doi.org/10.1016/j.nimb.2019.01.017.

[17] E. Viswanathan, D. Kanjilal, K. Sivaji, S. Ganapathy, Identification of sublattice damages in swift heavy ion irradiated n-doped 6h-sic polytype studied by solid state NMR, J. Phys. Chem. B. 115 (2011) 7766–7772. https://doi.org/10.1021/jp201367b.

[18] H.A.A. Abdelbagi, V.A. Skuratov, S. V. Motloung, E.G. Njoroge, M. Mlambo, J.B. Malherbe, J.H. O'Connell, T.T. Hlatshwayo, Effect of swift heavy ions irradiation in the migration of silver implanted into polycrystalline SiC, Nucl. Instruments Methods Phys. Res. Sect. B Beam Interact. with Mater. Atoms. 461 (2019) 201–209. https://doi.org/10.1016/j.nimb.2019.10.002.

[19] J.H. O'Connell, V.A. Skuratov, A.S. Sohatsky, J.H. Neethling, 1.2 MeV/amu Xe ion induced damage recovery in SiC, Nucl. Instruments Methods Phys. Res. Sect. B Beam Interact. with Mater. Atoms. 326 (2014) 337–340. https://doi.org/10.1016/j.nimb.2013.09.034.

[20] N. Daghbouj, B.S. Li, M. Callisti, H.S. Sen, M. Karlik, T. Polcar, Microstructural

evolution of helium-irradiated 6H–SiC subjected to different irradiation conditions and annealing temperatures: A multiple characterization study, Acta Mater. 181 (2019) 160–172. https://doi.org/10.1016/j.actamat.2019.09.027.

[21] A.J. Leide, R.I. Todd, D.E.J. Armstrong, Measurement of swelling-induced residual stress in ion implanted SiC, and its effect on micromechanical properties, Acta Mater. 196 (2020) 78–87. https://doi.org/10.1016/j.actamat.2020.06.030.

[22] T. Koyanagi, D.J. Sprouster, L.L. Snead, Y. Katoh, X-ray characterization of anisotropic defect formation in SiC under irradiation with applied stress, Scr. Mater. 197 (2021). https://doi.org/10.1016/j.scriptamat.2021.113785.

[23] S. Yang, S. Tokunaga, M. Kondo, Y. Nakagawa, T. Shibayama, Non-destructive evaluation of the strain distribution in selected-area He+ ion irradiated 4H-SiC, Appl. Surf. Sci. 500 (2020) 1–5. https://doi.org/10.1016/j.apsusc.2019.144051.

[24] A. Jankowiak, C. Grygiel, I. Monnet, Y. Serruys, C. Colin, S. Miro, L. Gelebart, L. Gosmain, J.M. Costantini, Advanced SiC fiber strain behavior during ion beam irradiation, Nucl. Instruments Methods Phys. Res. Sect. B Beam Interact. with Mater. Atoms. 314 (2013) 144–148. https://doi.org/10.1016/j.nimb.2013.04.031.

[25] I. Szlufarska, P. Voyles, K. Sridharan, Y. Katoh, Role of Defects in Swelling and Creep of Irradiated SiC, (2016). https://neup.inl.gov/SiteAssets/Final Reports/FY 2012/12-3357 NEUP Final Report.pdf.

[26] A. Jankowiak, C. Grygiel, I. Monnet, Y. Serruys, C. Colin, S. Miro, L. Gelebart, L. Gosmain, J.M. Costantini, Advanced SiC fiber strain behavior during ion beam irradiation, Nucl. Instruments Methods Phys. Res. Sect. B Beam Interact. with Mater. Atoms. 314 (2013) 144–148. https://doi.org/10.1016/j.nimb.2013.04.031.

[27] S. Biira, B.A.B. Alawad, H. Bissett, J.T. Nel, T.P. Ntsoane, T.T. Hlatshwayo, P.L. Crouse, J.B. Malherbe, Influence of the substrate gas-inlet gap on the growth rate, morphology and microstructure of zirconium carbide films grown by chemical vapour deposition, Ceram. Int. 43 (2017) 1354–1361. https://doi.org/10.1016/j.ceramint.2016.10.092.

[28] M. Ermrich, D. Opper, XRD for the analyst: getting acquainted with the principles, 2011.

[29] S. Biira, T.T. Hlatshwayo, P.L. Crouse, H. Bissett, T.T. Thabethe, M. Mlambo, J.B. Malherbe, Effect of the ZrCl 4 static vaporiser system and deposition time on growth characteristics of chemical vapour deposited zirconium carbide layers, Appl. Phys. A Mater. Sci. Process. 125 (2019). https://doi.org/10.1007/s00339-019-2490-3.

[30] G.K. Williamson, R.E. Smallman, III. Dislocation densities in some annealed and cold-worked metals from measurements on the X-ray Debye-Scherrer spectrum, Philos. Mag. 1 (1956) 34–46. https://doi.org/10.1080/14786435608238074.

[31] H. Harima, Raman scattering characterization on SiC, Microelectron. Eng. 83 (2006) 126–129. https://doi.org/10.1016/j.mee.2005.10.037.

[32] J.F. Ziegler, Interactions of ions with matter, Free Softw. (2015). https://doi.org/10.1007/3-540-29471-6_5.

[33] F. Gao, W.J. Weber, Cascade overlap and amorphization in (formula presented) Defect accumulation, topological features, and disordering, Phys. Rev. B - Condens. Matter Mater. Phys. 66 (2002) 1–10. https://doi.org/10.1103/PhysRevB.66.024106.

[34] Z. Xu, Z. He, Y. Song, X. Fu, M. Rommel, X. Luo, A. Hartmaier, J. Zhang, F. Fang, Topic review: Application of raman spectroscopy characterization in micro/nano-machining, Micromachines. 9 (2018) 1–23. https://doi.org/10.3390/mi9070361.

[35] V. Bratus, R. Melnyk, O. Kolomys, B. Shanina, V. Strelchuk, Photoluminescence spectroscopy of neutron-irradiated cubic SiC crystals, Mater. Sci. Forum. 740–742 (2013) 417–420. https://doi.org/10.4028/www.scientific.net/MSF.740-742.417.

[36] Z.C. Feng, C.C. Tin, R. Hu, J. Williams, Raman and Rutherford backscattering analyses of cubic SiC thin films grown on Si by vertical chemical vapor deposition, Thin Solid Films. 266 (1995) 1–7. https://doi.org/10.1016/0040-6090(95)06599-7.

[37] L.Z. Liu, J. Wang, X.L. Wu, T.H. Li, P.K. Chu, Longitudinal optical phonon–plasmon coupling in luminescent 3C–SiC nano-crystal films, Opt. Lett. 35 (2010) 4024. https://doi.org/10.1364/ol.35.004024.

[38] J.B. Malherbe, Diffusion of fission products and radiation damage in SiC, J. Phys. D. Appl. Phys. 46 (2013). https://doi.org/10.1088/0022-3727/46/47/473001.

[39] G.R. Wilkinson, Light Scattering in Solids III, 1983. https://doi.org/10.1080/716099630.

[40] G. Alfieri, T. Kimoto, First-principles study of Cl diffusion in cubic SiC, J. Appl. Phys. 113 (2013). https://doi.org/10.1063/1.4799194.

[41] S. Sorieul, J.M. Costantini, L. Gosmain, L. Thomé, J.J. Grob, Raman spectroscopy study of heavy-ion-irradiated α-SiC, J. Phys. Condens. Matter. 18 (2006) 5235–5251. https://doi.org/10.1088/0953-8984/18/22/022.

[42] A.J. Leide, M.J. Lloyd, R.I. Todd, D.E.J. Armstrong, Raman spectroscopy of ion irradiated SiC: chemical defects, strain, annealing, and oxidation, (2020). http://arxiv.org/abs/2004.14335.

[43] M.I. Idris, H. Konishi, M. Imai, K. Yoshida, T. Yano, Neutron Irradiation Swelling of SiC and SiCf/SiC for Advanced Nuclear Applications, Energy Procedia. 71 (2015) 328–336. https://doi.org/10.1016/j.egypro.2014.11.886.

[44] A. Henry, X. Li, H. Jacobson, S. Andersson, A. Boulle, D. Chaussende, E. Janzén, 3C-SiC heteroepitaxy on hexagonal SiC substrates, Mater. Sci. Forum. 740–742 (2013) 257–262. https://doi.org/10.4028/www.scientific.net/MSF.740-742.257.

[45] D.J. Sprouster, T. Koyanagi, E. Dooryhee, S.K. Ghose, Y. Katoh, L.E. Ecker, Microstructural evolution of neutron irradiated 3C-SiC, Scr. Mater. 137 (2017) 132–136. https://doi.org/10.1016/j.scriptamat.2017.02.030.

[46] T.T. Thabethe, T.T. Hlatshwayo, E.G. Njoroge, T.G. Nyawo, T.P. Ntsoane, J.B. Malherbe, Interfacial reactions and surface analysis of W thin film on 6H-SiC, Nucl. Instruments Methods Phys. Res. Sect. B Beam Interact. with Mater. Atoms. 371 (2016) 235–239. https://doi.org/10.1016/j.nimb.2015.10.063.

[47] S. Biira, P.L. Crouse, H. Bissett, T.T. Hlatshwayo, E.G. Njoroge, J.T. Nel, T.P. Ntsoane, J.B. Malherbe, The role of ZrCl 4 partial pressure on the growth characteristics of chemical vapour deposited ZrC layers, Ceram. Int. 43 (2017) 15133–15140. https://doi.org/10.1016/j.ceramint.2017.08.042.

[48] M.S.Ü. V. T. Srikar, Anna K. Swan, I. , Senior Member, andS. M.S. , Bennett B. Goldberg, Micro-Raman Measurement of Bending Stresses inMicromachined Silicon Flexures, J. MICROELECTROMECHANICAL Syst. 12 (2003) 779–787.

[49] and L.L. Stefan Rohmfeld, Martin Hundhausen, Quantitative evaluation of biaxial strain in epitaxial 3C-SiC layers on Si(100) substrates by Raman spectroscopy, J.

Appl. Phys. 91 (2002). https://doi.org/https://doi.org/10.1063/1.1427408.

[50] M.J. Madito, T.T. Hlatshwayo, V.A. Skuratov, C.B. Mtshali, N. Manyala, Z.M. Khumalo, Characterization of 167 MeV Xe ion irradiated n-type 4H-SiC, Appl. Surf. Sci. 493 (2019) 1291–1298. https://doi.org/10.1016/j.apsusc.2019.07.147.